Available online at www.sciencedirect.com
SCIENCE DIRECT®
International Journal of Heat and Mass Transfer 49 (2006) 307–316
International Journal of HEAT and MASS TRANSFER
www.elsevier.com/locate/ijhmt

A semiclassical two-temperature model for ultrafast laser heating

J.K. Chen [a,*], D.Y. Tzou [b], J.E. Beraun [a]

[a] Laser Effects Research Branch, Directed Energy Directorate, Air Force Research Laboratory, Kirtland AFB, NM 87117-5776, USA
[b] Department of Mechanical and Aerospace Engineering, University of Missouri-Columbia, Columbia, MO 65211, USA

Received 24 January 2005; received in revised form 22 June 2005
Available online 24 August 2005

Abstract

A semiclassical two-step heating model is proposed to investigate thermal transport in metals caused by ultrashort laser heating. Based on the Boltzmann transport equation, three equations of the conservation of number density, momentum and energy are derived for the electron subsystem. The thermal transport equation used for the phonon subsystem remains the same as that used in the phenomenological two-temperature (2T) model, including the energy exchange with hot electrons and the ultrafast thermal relaxation effect in general. The main difference between the semiclassical and the phenomenological 2T models is that the former includes the effects of electron drifting, which could result in significantly different electron and lattice temperature response from the latter for higher-intensity and shorter-pulse laser heating.

Keywords: Ultrashort laser heating; Boltzmann transport equation; Semiclassical two-temperature model; Electron drift velocity; Electron kinetic pressure

1. Introduction

Rapid advancement in ultrashort-pulsed lasers over the last decade has been driving a new research in many areas of physics, chemistry, materials, medicine, and engineering science. Among them, interaction of ultrashort-pulsed lasers with matter is a topic of numerous theoretical and experimental investigations [1–13, for example]. In the theoretical investigation several phenomenological two-temperature (2T) models [1–3] have been employed for solving ultrafast thermal response in the electrons and phonons (lattice), depending on laser pulse length and the type of materials.

In a non-uniformly heated conductor in the absence of current there arises an electric field [14]. If the electric field and the carrier gradient become excessively large, then non-equilibrium transport conditions will occur [15]. This could be particularly true for ultrashort-pulse laser heating due to the well-known fact that a tremendously sharp gradient of the electron temperature (or free electron density) is present in a small geometry encountered. In order to establish a model that can accurately describe the non-equilibrium electron effects, there is a need to examine the transport equations with the Boltzmann approximation.

* Corresponding author. Present address: Department of Mechanical and Aerospace Engineering, University of Missouri-Columbia, Columbia, MO 65211, USA. Tel.: +1 573 882 8159; fax: +1 573 884 5090.
E-mail address: chenjnk@missouri.edu (J.K. Chen).

0017-9310/$ - see front matter © 2005 Elsevier Ltd. All rights reserved.
doi:10.1016/j.ijheatmasstransfer.2005.06.022

Nomenclature

A_e, B_l	material constant for electron relaxation time
b	electron ballistic range
C	heat capacity
C_{e0}	electron heat capacity constant
C'_e	linear C_e assumed for $T_F/\pi^2 \leqslant T_e < T_F$
$\overline{E}$	electric field
e	charge of an electron
f	distribution function of electrons
G	electron–phonon coupling factor
G_{rt}	G at room temperature
H_m	fusion heat
$\tilde{I}$	unit dyad
K	thermal conductivity
k_B	Boltzmann constant
L	film thickness
m	mass of an electron
N	number density of atoms
$\mathbb{N}$	$= t_b V_F/\Delta x$
n	number density of electrons
$\tilde{P}$	electron kinetic pressure dyad
p	isotropic electron kinetic pressure
$\overline{Q}$	heat flux vector
q	number of total grid points
R	surface reflectivity
$\bar{r}$	position vector (x_i)
S	volumetric laser heat source
$\breve{S}$	modified laser heat source with electron ballistic motion
$\widehat{S}$	modified laser heat source with electron ballistic motion and thermalization
T	temperature
T_F	Fermi temperature
T_m	melting point
T_0	initial temperature
t	time
t_b	time of the electron ballistic motion
t_p	pulse duration defined as full width at half maximum
t_R	thermalization time of electrons
$u(t)$	unit step function
$\bar{u}$	velocity vector (u_i)
V_F	Fermi velocity
$\bar{v}$	mean (drift) velocity vector
Δx	grid spacing
x	direction of laser beam propagation

Greek symbols

β	electric field coefficient
χ, η	electron thermal conductivity constant
δ	optical penetration depth
ϕ	laser fluence
Λ	hot-electron blast force constant
μ_0	mobility of electrons at room temperature
θ_e	$=T_e/T_F$
θ_l	$=T_l/T_F$
τ	relaxation time
τ_{e-p}	energy relaxation time
τ_k	momentum relaxation time
ξ	electron energy density
Ψ	electron thermalization function

Subscripts and superscripts

c	collision
e	electron
j	grid point
l	lattice (phonon)
x	x-coordinate

In this paper a semiclassical 2T model is developed to investigate thermal transport in metals irradiated by ultrashort laser pulses. Three equations governing the conservation of number density, momentum and energy are derived for the electron subsystem from the first three moments of the Boltzmann transport equation. For the phonon subsystem, the thermal transport equation used is the same as that used in the phenomenological two-temperature (2T) model, including the energy exchange with hot electrons and the ultrafast thermal relaxation effect in general [3]. The temperatures in both the electron and lattice subsystems are solved simultaneously with a finite difference method. The main difference between the semiclassical and the phenomenological 2T models is that the former includes the effects of the electron drift velocity, which is caused by the resulting electric field and hot-electron kinetic pressure. In addition to the diffusion of electron energy, the drifting of electrons could play an important role in the thermal transport in ultrafast laser heating. Numerical analysis is performed for gold films. The results are compared with the phenomenological 2T model as well as the experimental data available in the open literature.

2. Semiclassical two-temperature model

The phenomenological, dual-hyperbolic 2T model proposed by Chen and Beraun [3] for ultrafast laser–material interactions is given as

$$C_e\frac{\partial T_e}{\partial t} = -\nabla\cdot\overline{Q}_e - G(T_e - T_l) + S(\bar{r},t) \tag{1}$$

$$\tau_e\frac{\partial \overline{Q}_e}{\partial t} + \overline{Q}_e = -K_e\nabla T_e \tag{2}$$

$$C_l\frac{\partial T_l}{\partial t} = -\nabla\cdot\overline{Q}_l + G(T_e - T_l) \tag{3}$$

$$\tau_l\frac{\partial \overline{Q}_l}{\partial t} + \overline{Q}_l = -K_l\nabla T_l \tag{4}$$

For pure metals, heat conduction in the lattice is small compared to that in the electrons. Therefore, $\overline{Q}_l$ in Eqs. (3) and (4) are often neglected. In that case the above dual-hyperbolic model is reduced to the hyperbolic 2T model [2]. By further letting τ_e in Eq. (2) be zero, the hyperbolic 2T model is reduced to the parabolic 2T model [1]. Since the electron relaxation time (τ_e) is shorter than several tens femtoseconds (fs) for metals, the difference among the three models would be insignificant provided that laser pulses are much longer than τ_e [16].

To establish a model that is able to describe the non-equilibrium electron effects more accurately, a set of the semiclassical transport equations are formulated below to accommodate the electron concentration, drifting (mean) velocity, and average energy based on the Boltzmann transport equation. Let $f(\bar{r},\bar{u},t)$ be a distribution function of electrons at time t in the phase space with position vector ($\bar{r}$) and velocity vector ($\bar{u}$). If the Lorentz force due to magnetic fields is neglected, the Boltzmann transport equation for electrons is in the form

$$\frac{df}{dt} = \frac{\partial f}{\partial t} + \bar{u}\cdot\nabla_r f + \frac{e}{m}\overline{E}\cdot\nabla_u f = \left(\frac{\partial f}{\partial t}\right)_c \tag{5}$$

where the del operators $\nabla_r = \partial/\partial x_i$ and $\nabla_u = \partial/\partial u_i$ (the index $i = 1,2,3$ refers to the direction); $e\overline{E}/m$ is the Lorentz force resulting from the electric field. The total derivative df/dt is evaluated along the trajectory $(\bar{r}(t),\bar{u}(t))$ in the absence of collision. The term $(\partial f/\partial t)_c$ is the time rate of change of f due to the electron collision.

For convenience, the electron number density $n(\bar{r},t)$, mean velocity vector $\bar{v}(\bar{r},t)$, kinetic pressure dyad $\widetilde{P}(\bar{r},t)$, and energy flux vector $\overline{Q}(\bar{r},t)$ in the entire velocity space are defined here by averaging the various moments of the phase space distribution function [17]:

$$n(\bar{r},t) = \int f(\bar{r},\bar{u},t)\,d\bar{u} \tag{6}$$

$$\bar{v}(\bar{r},t) = \frac{1}{n}\int \bar{u}f(\bar{r},\bar{u},t)\,d\bar{u} \tag{7}$$

$$\widetilde{P}(\bar{r},t) = m\int(\bar{u}-\bar{v})(\bar{u}-\bar{v})f(\bar{r},\bar{u},t)\,d\bar{u} \tag{8}$$

$$\overline{Q}(\bar{r},t) = \frac{m}{2}\int(\bar{u}-\bar{v})\cdot(\bar{u}-\bar{v})(\bar{u}-\bar{v})f(\bar{r},\bar{u},t)\,d\bar{u} \tag{9}$$

The continuity equation for the electron number density can be derived by integrating the Boltzmann transport equation (5) over velocities,

$$\int\left(\frac{\partial f}{\partial t} + \bar{u}\cdot\nabla_r f + \frac{e}{m}\overline{E}\cdot\nabla_u f\right)d\bar{u} = \int\left(\frac{\partial f}{\partial t}\right)_c d\bar{u} \tag{10}$$

Since $\bar{r}$ and $\bar{u}$ are independent, the above equation is simplified to

$$\frac{\partial n}{\partial t} + \nabla_r\cdot(n\bar{v}) = \left(\frac{\partial n}{\partial t}\right)_c \tag{11}$$

The third term in Eq. (10) vanishes due to the fact that $f\to 0$ as $|\bar{v}|\to\infty$ and the condition that $\overline{E}$ is independent of $\bar{u}$.

Multiplying Eq. (5) by the velocity $\bar{u}$ and integrating the equation over the velocity space results in the equation of the conservation of momentum for the electron gas

$$m\frac{\partial\bar{v}}{\partial t} + m\bar{v}\cdot\nabla_r\bar{v} - e\overline{E} + \frac{1}{n}\nabla_r\cdot\widetilde{P} = m\left(\frac{\partial\bar{v}}{\partial t}\right)_c \tag{12}$$

Assuming an isotropic Maxwell–Boltzmann distribution of peculiar velocities, the electron kinetic pressure is isotropic, i.e., $\widetilde{P} = p\tilde{I} = nk_BT_e\tilde{I}$ [17]. The electric field generated in a non-uniformly heated conductor in the absence of current is $\overline{E} = \beta\nabla T_e$ with $\beta = -1.42\times 10^{-4}(T_e/T_F)$ V/K for free electrons [14]. The collision term $m(\partial\bar{v}/\partial t)_c$ represents the time rate of change of momentum density due to intraband collisions and generation-recombination processes and is approximated by [15]

$$m\left(\frac{\partial\bar{v}}{\partial t}\right)_c = -m\frac{\bar{v}}{\tau_k} \tag{13}$$

where $\tau_k = m\mu_0T_l/eT_e$ is the momentum relaxation time [18].

It is well-known that only those electrons in states within the energy range k_BT can be excited thermally at temperature T. If one atom can give one valence electron to the free electron gas, then the number density of the excited electrons at temperatures $T_e \ll T_F$ is given by [19]

$$n = \frac{1}{3}\pi^2N\frac{T_e}{T_F} \tag{14}$$

The renowned linear relationship of the electron heat capacity is thus derived

$$C_e = \frac{3}{2}nk_B = \frac{1}{2}\pi^2Nk_B\frac{T_e}{T_F} = C_{e0}T_e \tag{15}$$

with the constant $C_{e0} = \pi^2Nk_B/2T_F$. The electron kinetic pressure, $p = nk_BT_e$, can be re-expressed in terms of C_{e0} and T_e

$$p = \frac{2}{3}C_{e0}T_e^2 \tag{16}$$

Thus,

$$\nabla_r \cdot \widetilde{P} = 2nk_B \nabla T_e = \nabla\left(\frac{2}{3} C_{e0} T_e^2\right) \tag{17}$$

The term $\nabla_r \cdot \widetilde{P}$ derived above is the so-called hot-electron blast force $\nabla(\Lambda T_e^2)$ that was derived by Falkovsky and Mishchenko in 1999 [20]. Because it was too difficult to solve the coupled non-linear Boltzmann and thermo-conductivity equations, the constant Λ was approximated to be gC_{e0} with $g \sim 1$ based on the dominant contribution from the local equilibrium partition function [20]. In this work, the constant Λ is exactly derived with $g = 2/3$. It should be pointed out here that as described by Eqs. (14)–(17), the hot-electron blast force derived by Falkovsky and Mishchenko is only adequate for $T_e < 0.1T_F$. For higher temperatures, the electric kinetic pressure is $p = nk_B T_e = 2C_e T_e/3$. Thus, a general form of the hot-electron blast force should be $2\nabla(C_e T_e)/3$. Fig. 1 gives the temperature-dependent heat capacity of electrons for gold used in this study. In view of the result [21], the relations $C_e = 2C_{e0}T_e/3 + C'_e/3$ for $T_F/\pi^2 \leqslant T_e < 3T_F/\pi^2$ and $C_e = Nk_B + C'_e/3$ for $3T_F/\pi^2 \leqslant T_e < T_F$ in Fig. 1 are approximated.

Substitution the relationships $\nabla_r \cdot \widetilde{P} = \nabla_r(nk_B T_e)$, $\overline{E} = \beta \nabla T_e$, and $(\partial \bar{v}/\partial t)_c = eT_e \bar{v}/\mu_0 T_l$ into Eq. (12) yields

$$m\frac{\partial \bar{v}}{\partial t} + m\bar{v} \cdot \nabla_r \bar{v} + \left[k_B\left(1 + \frac{T_e}{C_e}\frac{\partial C_e}{\partial T_e}\right) - e\beta\right]\nabla T_e = -\frac{eT_e \bar{v}}{\mu_0 T_l} \tag{18}$$

For low temperatures $\frac{T_e}{C_e}\frac{\partial C_e}{\partial T_e} = 1$ since $C_e = C_{e0}T_e$. Eq. (18) indicates that the electron drift velocity $\bar{v}$ is governed by the electron temperature distribution.

Similar to the derivation of the momentum equation, the energy equation can be obtained by multiplying Eq. (5) by the kinetic energy, $m\bar{u} \cdot \bar{u}/2$. Averaging the result over the entire velocity space and utilizing the continuity and momentum conservation conditions lead to

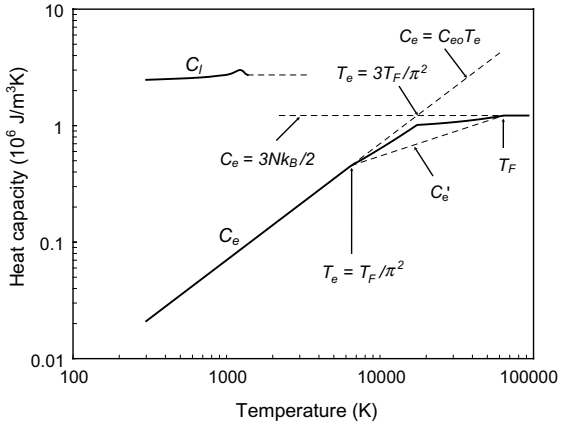

Fig. 1. Heat capacity of gold.

$$\frac{\partial \xi}{\partial t} + \bar{v} \cdot \nabla_r \xi + \frac{1}{n}\nabla_r \cdot (nk_B T_e \bar{v}) + \frac{1}{n}\nabla_r \cdot \overline{Q}_e - e\beta \bar{v} \cdot \nabla T_e = \left(\frac{\partial \xi}{\partial t}\right)_c \tag{19}$$

where $\xi = m|\bar{v}|^2/2 + 3k_B T_e/2$ is the electron energy density. The collision term, which is the time rate of change of electron energy density due to electron–phonon scattering and generation-recombination events, is approximated as $(\partial\xi/\partial t)_c = (\xi - \xi_l)/\tau_{e-p}$ with ξ_l denoting the equilibrium energy when $T_e = T_l$ and τ_{e-p} being the characteristic time for electrons and phonons to reach equilibrium [15]. By making use of the momentum equation, Eq. (19) is reduced to

$$C_e\left(\frac{\partial T_e}{\partial t} + \bar{v} \cdot \nabla_r T_e + \frac{2}{3}T_e \nabla_r \cdot \bar{v}\right) + \nabla_r \cdot \overline{Q}_e = C_e\left(\frac{\partial T_e}{\partial t}\right)_c \tag{20}$$

The term $C_e(\partial T_e/\partial t)_c$ in Eq. (20) is equal to $C_e(T_e - T_l)/\tau_{e-p}$, which represents the time rate of thermal energy exchange between the electrons and lattice. Along with the optical-electron scattering due to laser excitation the energy equation (20) becomes

$$C_e\left(\frac{\partial T_e}{\partial t} + \bar{v} \cdot \nabla_r T_e + \frac{2}{3}T_e \nabla_r \cdot \bar{v}\right) + \nabla_r \cdot \overline{Q}_e = -G(T_e - T_l) + S(\bar{r}, t) \tag{21}$$

where $G = C_e/\tau_{e-p}$ is the electron–phonon coupling factor. The electron–phonon thermalization time can be determined with given G and C_e; for example, $\tau_{e-p} \sim 1$ ps for metals at rt [2].

The semiclassical 2T model derived above includes: Eqs. (18) and (21), the equations of the conservation of momentum and energy for the electron subsystem; Eq. (3), the equation of energy balance for the lattice subsystem; and Eqs. (2) and (4), the constitutive equations for heat fluxes in the electrons and lattice. For a 1D transport problem, for instance, the above five equations are satisfied by the five unknowns, Q_{ex}, T_e, v_x, Q_{lx}, and T_l. The phenomenological dual-hyperbolic 2T models, on the other hand, involve four unknowns, Q_{ex}, T_e, Q_{lx} and T_l, to be solved. The difference between the present semiclassical and the phenomenological 2T models is thus clear. The former not only includes two extra terms in the energy balance equation for the electron subsystem but also describe the electron drift velocity in the momentum equation. Like the phenomenological 2T models, the semiclassical model can be simplified under the assumptions $\overline{Q}_l = 0$ and/or $\tau_e = 0$.

As described by the momentum equation (18), the electron drift velocity depends on the temperature field. Noting the dependence of laser pulse length and fluence for the electron temperature, it is observed from Eqs. (18) and (21) that the shorter and the more intense a laser pulse is, the higher the drift velocity would be

and, consequently, the more the distinction between the semiclassical and phenomenological 2T models would exhibit. The conjecture will be confirmed numerically later.

3. Solution algorithm

A 1D problem is numerically analyzed for pure metals in this work since ultrashort-pulsed laser spot sizes are often much larger than the depth of the thermally affected zone for the interaction time of interest [22]. The 1D version of the governing equations (2) and (3) with $\overline{Q}_l = 0$, (18) and (21) together with the following initial and boundary conditions are solved with a central difference method [16]:

$$T_e(x,0) = T_l(x,0) = T_0; \quad v_x(x,0) = 0 \tag{22}$$

$$Q_{ex}(0,t) = Q_{ex}(L,t) = 0 \tag{23}$$

where T_0 is set at 300 K.

The laser heat source which has been widely used in 2T models is expressed as

$$S(x,t) = -\sqrt{\frac{4\ln 2}{\pi}}\frac{(1-R)\phi}{\delta t_p} \times \exp\left\{-\frac{x}{\delta} - 4\ln 2\left[\left(\frac{t-2t_p}{t_p}\right)^2\right]\right\} \tag{24}$$

Lasing is assumed to start at $t = 0$ and end at $t = 4t_p$. The laser energy outside this period of time is neglected since it is too small to significantly alter the result. It should be noted that an intrinsic assumption that the excited electrons are immediately and fully thermalized is applied when Eq. (24) is directly input to the energy equation (21).

Immediately after a metal solid is illuminated by a sub-picosecond (ps) laser pulse, while the excited electrons are still highly non-equilibrium, two competing processes take place. The non-thermalized electrons move ballistically with a velocity close to the Fermi velocity. Through collision, meanwhile, those non-thermalized electrons continue to thermalize into a Fermi–Dirac distribution in which the electron temperature can be measurable. It takes a finite period of time for the excited electrons to travel ballistically and complete the thermalization. Therefore, the laser heat source term used in ultrafast 2T models should differ from that described by Eq. (24). The other factor that may also play a role in re-distributing the absorbed photon energy is the change of the thermalized electron distribution due to the electron drifting. However, this effect is neglected in this work due to the fact that the electron drift velocity is much smaller than the ballistic velocity.

To better match the theoretical electron temperature with the measured surface reflectivity, an effective absorption depth that combines the optical penetration depth (δ) and an electron ballistic range (b) was introduced [22–24]. For instance, an electron ballistic range of 105 nm was assumed for gold, based on the postulation that the excited, non-equilibrium electrons could penetrate into the non-excited spatial region at the Fermi velocity for about 100 fs [23]. With this approach the re-distributed laser heat source remains exponential, described by $\exp[-x/(\delta + b)]$. Instead of imposing a ballistic range on the optical penetration depth, we allow the non-thermal equilibrium electrons to move randomly at the Fermi velocity for a finite period of time (t_b). Upon the excitation by a laser pulse, the spatial distribution of the absorbed photon energy is given by Eq. (24). The absorbed energy then attenuates as the non-thermalized electrons propagate. For a grid spacing Δx, the time interval for the excited electrons to travel from a grid point to its neighbor points is $\Delta x/V_F$. Thus, the spatial distribution of the laser heat source after each time interval becomes: $\breve{S}_j = (\breve{S}_{j-1} + \breve{S}_{j+1})/2$ for interior points $(j = 2,\ldots,q-1)$ and $\breve{S}_1 = (\breve{S}_1 + \breve{S}_2)/2$ and $\breve{S}_q = (\breve{S}_{q-1} + \breve{S}_{q+1})/2$ for the boundary points, where $\breve{S}_j = \breve{S}(x_j,t)$ for these terms on the left-hand sides, $\breve{S}_j = \breve{S}(x_j,t-\Delta t)$ for those on the right-hand sides, and $\breve{S}_j(x_j,0) = S(x_j,0)$, $j = 1,2,\ldots,q$. The above re-distribution of the laser heat source continues for $\mathbb{N}$ times with $\mathbb{N}$ being determined from the relationship $\mathbb{N}\Delta x/V_F = t_b$.

On the other hand, energy transfer from the non-thermal part of the excited free electrons into the Fermi–Dirac distribution takes place until the thermalization process is complete. To accommodate the delayed rise time of the electron temperature due to the build up of the Fermi distribution, a system response function was introduced [24,25]. In this work, the function proposed by Ibrahim et al. [24] is considered for accounting the delayed thermalization for the electrons excited at time t'

$$\Psi(t,t') = u(t-t')\left\{1 - \exp\left[-\left(\frac{t-t'}{t_R}\right)^2\right]\right\} \tag{25}$$

According to Eq. (25), completion of the thermalization is 0%, 63.2%, and 99.99% at $t - t' = 0$, t_R and $3t_R$, respectively.

By including both the electron ballistic motion and the thermalization effects, the re-distributed laser heat source ($\widehat{S}$) used in the 2T models becomes

$$\widehat{S}(x,t) = \sum_{t'=0}^{t'=t} \breve{S}(x,t')[\Psi(t,t') - \Psi(t-\Delta t,t')] \tag{26}$$

The thermal conductivity and relaxation time of electrons and the electron–phonon coupling factor used in this study all are temperature dependent [26]:

$$K_e = \chi \frac{(\theta_e^2 + 0.16)^{5/4}(\theta_e^2 + 0.44)\theta_e}{(\theta_e^2 + 0.092)^{1/2}(\theta_e^2 + \eta\theta_l)} \quad (27)$$

$$\tau_e(T_e, T_l) = \frac{1}{A_e T_e^2 + B_l T_l} \quad (28)$$

$$G = G_{rt}\left[\frac{A_e}{B_l}(T_e + T_l) + 1\right] \quad (29)$$

When a laser pulse length is much longer than the electron relaxation time, the electron relaxation term $\tau_e \partial \overline{Q}_e/\partial t$ in Eq. (2) can be neglected. It, however, was found from our numerical simulation that a much smaller time increment is needed for advancing the solution when this term is dropped off. For saving the computer time, it is retained in the analysis even though the laser pulse durations are much longer than τ_e.

4. Numerical results

The numerical analysis was performed for gold with a finite difference model composing of equally spaced grid points. The material properties used are as follows [19,26] unless otherwise mentioned: $C_{e0} = 70\ \mathrm{J\ m^{-3}\ K^{-2}}$, $K_l = 0$, $T_m = 1337\ \mathrm{K}$, $H_m = 6.275 \times 10^4\ \mathrm{J\ kg^{-1}}$, $T_F = 6.4 \times 10^4\ \mathrm{K}$, $N = 5.9 \times 10^{28}\ \mathrm{m^{-1}}$, $\mu_0 = 4.8 \times 10^{-3}\ \mathrm{m^2\ s^{-1}\ V^{-1}}$, $R = 0.93$, $\alpha = 15.3\ \mathrm{nm}$, $A_e = 1.2 \times 10^7\ \mathrm{K^{-2}\ s^{-1}}$, $B_l = 1.23 \times 10^{11}\ \mathrm{K^{-1}\ s^{-1}}$, $G_{rt} = 2.2 \times 10^{16}\ \mathrm{W\ m^{-3}\ K^{-1}}$, $\chi = 353\ \mathrm{W\ m^{-1}\ K^{-1}}$, $\eta = 0.16$, and $t_b = 100\ \mathrm{fs}$. The solid line of C_l given in Fig. 1 is calculated from the relationship $C = C_e + C_l$ with C being the bulk heat capacity. Resolution of the model and the time increment was first studied with three sizes of grid spacing, 0.5, 1.0 and 2.0 nm. It was found that the grid size of 1 nm is adequate to resolve the problem. Therefore, uniform-mesh models with grid points of 1 nm apart were employed in the following. The time increment used was 0.5×10^{-16} s except for the 800-ps laser pulse case, for which the time increment was increased to 1.0×10^{-15} s.

Fig. 2 shows the normalized change of the electron temperature at the front surface ($x = 0$) of an 80-nm gold film illuminated by a 2.8 mJ/cm^2, 800-nm, 150-fs laser pulse. The values of R, α and t_R used in this calculation were 0.967, 12.7 nm and 500 fs, respectively. The experimental temperature data was deduced from the measured reflectivity [24] with the linear relationship $\Delta T_e \sim \Delta R$. For comparison, the result computed with $t_R = 0$ (i.e. all the excited electrons complete thermalization instantaneously) and that obtained from the phenomenological 2T model with $t_R = 500$ fs are also presented in the figure. The simulated maximum electron temperature was 335.9 K for the case of $t_R = 500$ fs and 357.7 K for $t_R = 0$, occurring at 0.988 ps and 0.358 ps, respectively. As shown in Fig. 2, it is clear that the case of $t_R = 0$ fails to capture the electron temperature response for the first several hundred femtoseconds.

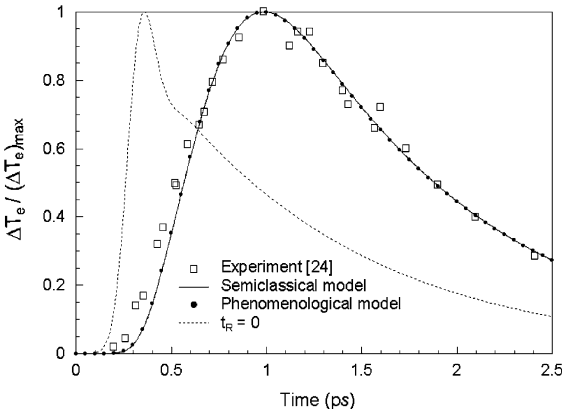

Fig. 2. Comparison of the change in electron temperature at the front surface of an 80-nm gold film irradiated by a 2.8 mJ/cm^2, 800 nm, 150-fs laser pulse.

On the other hand, the result computed with $t_R = 500$ fs agrees very well with the experimental data. It is worth noting again the electron thermalization effects on the delayed rise time of electron temperature and the reduction of the maximum temperature. The reason for such a time delay and the reduction is the prolonged energy transfer from the non-thermal part of the excited free electrons into the Fermi–Dirac distribution. The delayed response is accommodated by Eq. (26). Further investigation with different values of the thermalization time t_R (not shown here for brevity) proved that the maximum surface reflectivity decreases with the increase of t_R, according to the relationship $\Delta R \sim \Delta T_e$. It is also seen in Fig. 2 that at this low level of laser fluence the difference between the semiclassical and the phenomenological 2T models is negligible.

Fig. 3 shows the normalized change of the electron temperature at the front surface of a 100-nm gold film

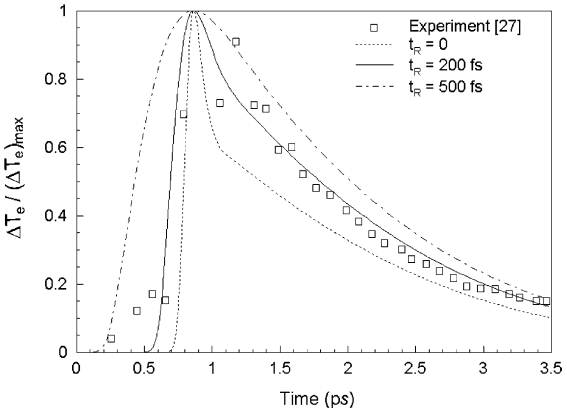

Fig. 3. Comparison of the change in electron temperature at the front surface of a 100-nm gold film irradiated by a 13.4 mJ/cm^2, 560-nm, 100-fs laser pulse.

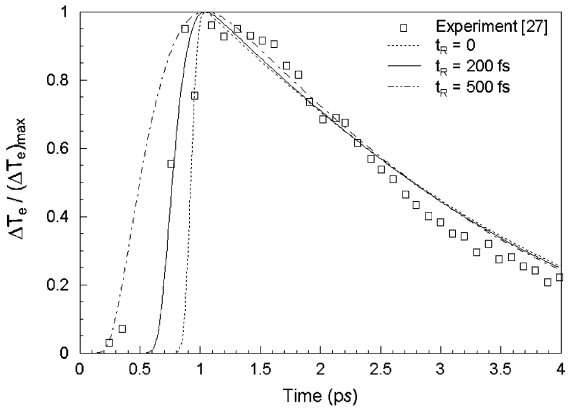

Fig. 4. Comparison of the change in electron temperature at the front surface of a 20-nm gold film irradiated by a 13.4 mJ/cm^2, 560-nm, 100-fs laser pulse.

subjected to a 13.4 mJ/cm^2, 630-nm, 100-fs laser heating. Three electron thermalization times, $t_R = 0$, 200 fs and 500 fs, were examined. For ease of comparison all the results are shifted so that the peak electron temperatures appear at the same instance of time. The calculated times when the maximum temperatures are reached are 0.244, 0.460 and 0.862 ps, respectively. Apparently, the result obtained with $t_R = 200$ fs is in good correlation with the experimental data over the entire time history [27], compared to the other two cases. The same conclusion can be made for the 20-nm gold film (see Fig. 4). In this case, the calculated peak temperatures occur at 0.304, 0.599 and 1.042 ps, respectively.

The effect of the film thickness on the rise of electron temperature at the heated surface is shown in Fig. 5. In view of the results in Figs. 3 and 4, a value of $t_R = 200$ fs was used in this analysis. It appears from Fig. 5 that increasing sample thickness decreases the delayed rise time of the electron temperature, up to the film thickness of 100 nm. The other finding is that the temperature decay time decreases as the sample thickness increases, up to the film thickness of 500 nm.

In the above analysis, the absorbed laser fluence is 0.938 mJ/cm^2 for the 13.4 mJ/cm^2, 630-nm, 100-fs laser heating (Figs. 3 and 4) and is only 0.0924 mJ/cm^2, one order lower, for the 2.8 mJ/cm^2, 800-nm, 150-fs laser heating (Fig. 2). The results in Figs. 2–4 reveal that the electron thermalization time in the former is about 200 fs, a 60% reduction from that in the latter. This suggests that the electron thermalization time decrease with the increase of laser fluence, which is consistent with the previous observation [25]. It is thus expected that the excited electrons would thermalize very fast should laser fluences be sufficiently high. Therefore, modification of the laser heat source due to electron thermalization is neglected in the following simulations since the fluences considered are much higher than those studied above.

Fig. 6 shows the electron and lattice temperatures at the heated surface of a 1.0-μm gold film illuminated by a 0.1 J/cm^2, 630-nm, 100-fs laser pulse. At this level of laser fluence, the difference between the semiclassical and phenomenological 2T models is discernable although it is immaterial. A pronounced distinction is seen in Fig. 7 for the higher fluence 1.0 J/cm^2. These results confirm the conjecture that the more intense the laser pulse, the more the distinction between the two models.

The electron temperature distribution provides useful information for the electric field and the shock wave generation in the material and is plotted in Fig. 8 for a 1.0-μm gold film heated by a 1.0 J/cm^2, 630-nm, 100-fs laser pulse. For clarity, only the result over the region of $x = 0$–0.3 μm is presented here. Fig. 9 depicts the resulting electric field ($E_x = \beta T_{e,x}$). The electric field

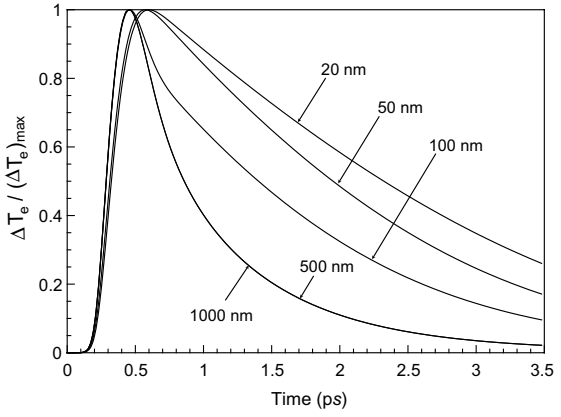

Fig. 5. Thickness effect on the electron temperature at the front surface of gold films irradiated by a 13.4 mJ/cm^2, 560-nm, 100-fs laser pulse.

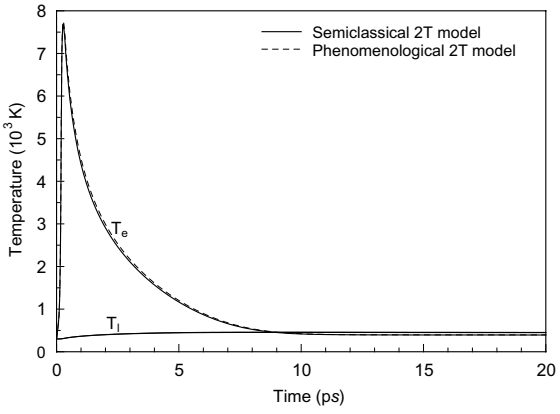

Fig. 6. Time history of temperatures at the front surface of a 1.0-μm gold film heated with a 0.1 J/m^2, 560-nm, 100-fs laser pulse.

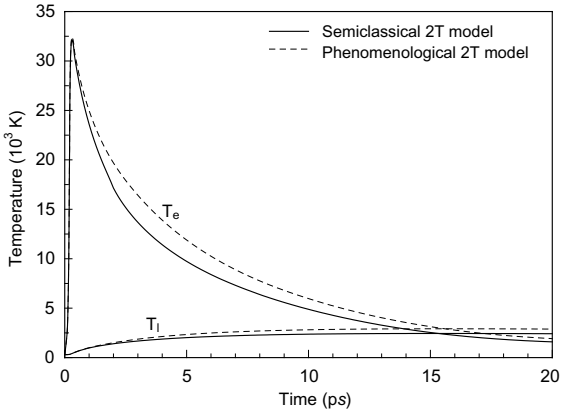

Fig. 7. Time history of temperatures at the front surface of a 1.0-μm gold film heated with a 1.0 J/m^2, 560-nm, 100-fs laser pulse.

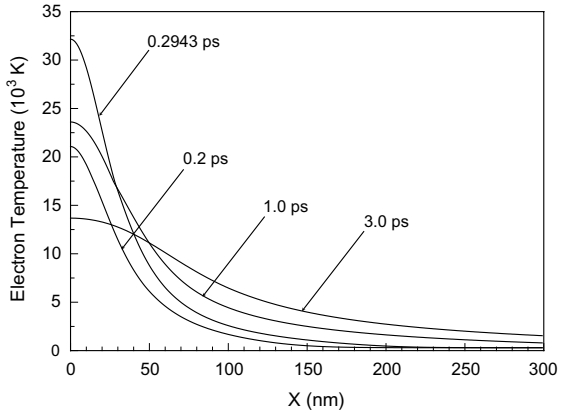

Fig. 8. Electron temperature distribution over the region of $x = 0$–0.3 μm in a 1.0-μm medium irradiated with a 1.0 J/m^2, 560-nm, 100-fs laser pulse.

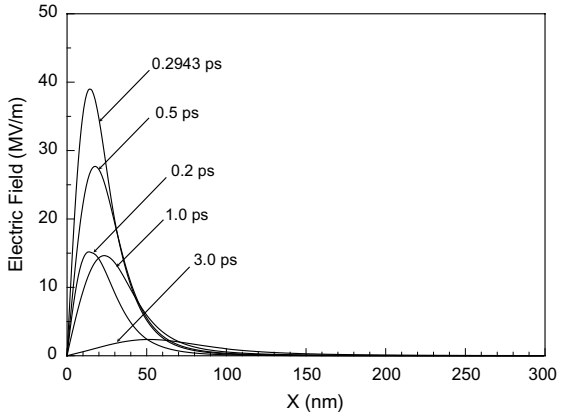

Fig. 9. Electric field over the region of $x = 0$–0.3 μm in a 1.0-μm medium irradiated with a 1.0 J/m^2, 560-nm, 100-fs laser pulse.

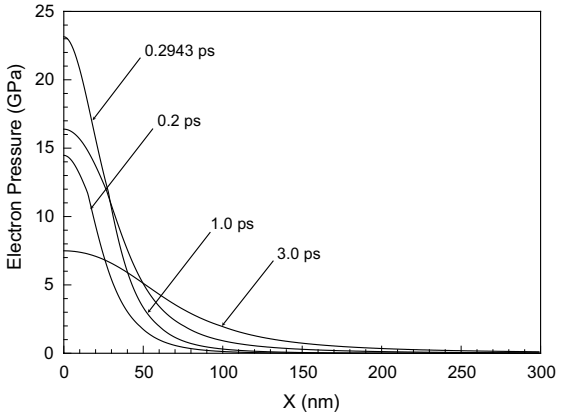

Fig. 10. Electric kinetic pressure distribution over the region of $x = 0$–0.3 μm in a 1.0-μm medium irradiated with a 1.0 J/m^2, 560-nm, 100-fs laser pulse.

intensity is about 39 MV/m when the electron temperature peaks at $t = 0.2943$ ps. The induced electron kinetic pressure ($p = 2C_eT_e/3$) is shown in Fig. 10. The maximum pressure is 23.1 GPa, approximately 19 times the ultimate strength of gold (1.24 GPa). Since the characteristic diffusion velocity of electron thermal energy, $(K_e/C_e\tau_e)^{1/2}$, is much higher than the speed of sound, the lattice motion is essentially initiated by the excessive pressure of the hot-electron gas during the early time. The resulting stresses in the lattice are subjected to the electron kinetic pressure, thermal expansion, and boundary conditions. The role that the hot-electron blast force, ∇p, could play in destroying the cold lattice was briefly discussed in Refs. [6,20]. Further investigation of the electric field and the electron kinetic pressure on the ultrashort laser ablation is suggested.

Fig. 11 compares the simulated damage fluence threshold with the experimental data [28] for gold irradi-

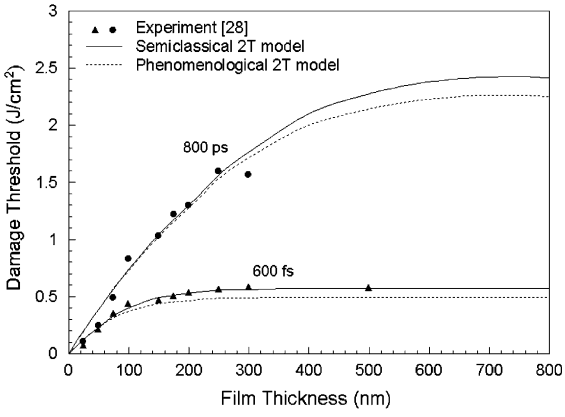

Fig. 11. Comparison of the simulated and measured damage thresholds for a gold film heated with 600-fs and 800-ps laser pulses.

ated by two 1053-nm lasers of different pulse lengths, 600 fs and 800 ps, respectively. The measured damage thresholds were determined based on the visible modification to the front surface. Accordingly, it is assumed here that initiation of damage occurs when the front surface completes the solid-to-liquid phase change (melting). At this wavelength the skin depth is 3 nm. The surface reflectivity used in the simulation is 0.9260 for the 600-fs pulse and 0.9546 for the 800-ps pulse. It can be seen from Fig. 11 that the semiclassical 2T model is in good agreement with the measurement for both laser pulses. The phenomenological 2T model, on the other hand, results in slightly lower damage thresholds. For the case of the 800-nm film heated by the 600-fs laser pulse, for example, the damage threshold obtained from the semiclassical model is about 12% higher than that obtained from the phenomenological model. It reduces to 7% for the longer, 800-ps pulse. This confirms the conjecture that the shorter the laser pulses, the more the distinction between the two models.

As shown in the energy equation (21), the two terms that involve the electron drift velocity and are excluded in conventional 2T models are $\bar{v} \cdot \nabla_r T_e$ and $2T_e \nabla_r \cdot \bar{v}/3$. Our numerical results demonstrate that the latter has much more impact on the change of electron temperature than the former. The difference of the impacts is on the order of six (6). Accordingly, the term $\bar{v} \cdot \nabla_r T_e$ can be neglected without significant change of the result.

5. Conclusions

A semiclassical two-temperature model was formulated to investigate thermal transport in metals heated by ultrashort-pulsed lasers. The difference between the semiclassical and phenomenological 2T models is that the former includes two extra terms in the equation of energy balance in the electron subsystem, involving the electron drift velocity that is caused by the generated electric field and the electron kinetic pressure as described in the momentum equation. The volumetric laser heat source used in the model was modified for accommodating the electron ballistic motion and the delayed rise time of the electron temperature. The temperature fields in the electrons and lattice were solved with the equations of the conservation of momentum and energy in electron subsystem and the equation of heat conduction in the lattice subsystem. Numerical analysis was performed for gold films. It was shown that for higher-intensity and shorter-laser pulses, the semiclassical 2T model could result in different thermal response than the phenomenal 2T model. It was also found that the damage fluence threshold simulated with the semiclassical 2T model correlates very well with the experimental data for gold irradiated by ultrashort (600 fs) and longer (800 ps) laser pulses.

References

[1] S.I. Anisimov, B.L. Kapeliovich, T.L. Perel'man, Electron emission from metal surfaces exposed to ultrashort laser pulses, Sov. Phys. JETP 39 (1974) 375–377.
[2] T.Q. Qiu, C.L. Tien, Heat transfer mechanisms during short-pulse laser heating of metals, ASME J. Heat Transfer 115 (1993) 835–841.
[3] J.K. Chen, J.E. Beraun, Numerical study of ultrashort laser pulse interactions with metal films, Numer. Heat Transfer A 40 (2001) 1–20.
[4] S. Nolte, C. Momma, H. Jacobs, A. Tunnermann, B.N. Chichkov, B. Wellegehausen, H. Welling, Ablation of metals by ultrashort laser pulses, J. Opt. Soc. Am. B 14 (1997) 2716–2722.
[5] D.Y. Tzou, J.E. Beraun, J.K. Chen, Ultrafast deformation in femtosecond laser heating, ASME J. Heat Transfer 124 (2002) 284–292.
[6] J.K. Chen, J.E. Beraun, L.E. Grimes, D.Y. Tzou, Modeling of femtosecond laser-induced nonequilibrium deformation in metal films, Int. J. Solids Struct. 39 (2002) 3199–3216.
[7] X. Wang, X. Xu, Thermoelastic wave in metals induced by ultrafast laser pulses, J. Therm. Stresses 25 (2002) 457–473.
[8] D.A. Willis, X. Xu, Heat transfer and phase change during picosecond laser ablation of nickel, Int. J. Heat Mass Transfer 45 (2002) 3911–3918.
[9] C. Schäfer, H.M. Urbassek, L.V. Zhigilei, Metal ablation by picosecond laser pulses: a hybrid simulation, Phys. Rev. B 66 (2002) 115404.
[10] J.K. Chen, J.E. Beraun, Modeling of ultrashort laser ablation of gold films in vacuum, J. Opt. A 5 (2003) 168–173.
[11] S.R. Vatsya, K.S. Virk, Solution of two-temperature thermal diffusion model of laser–metal interactions, J. Laser Appl. 15 (2003) 273–278.
[12] C. Cheng, X. Xu, Molecular dynamic study of volumetric phase change induced by a femtosecond laser pulse, Appl. Phys. A 79 (2004) 761–765.
[13] E. Leveugle, D.S. Ivanov, L.V. Zhigilei, Photomechanical spallation of molecular and metal targets: molecular dynamics study, Appl. Phys. A 79 (2004) 1643–1655.
[14] N.W. Ashcroft, N.D. Mermin, Solid State Physics, Saunders College, Philadelphia, 1976.
[15] C.M. Snowden, Introduction to Semiconductor Device Modelling, World Science, Singapore, 1986.
[16] J.K. Chen, J.E. Beraun, C.L. Tham, Investigation of thermal response caused by pulse laser heating, Numer. Heat Transfer A 44 (2003) 705–722.
[17] W.L. Kruer, The Physics of Laser Plasma Interactions, Addison-Wesley, Redwood City, CA, 1988.
[18] G. Baccarani, M.R. Wordeman, An investigation of steady-state velocity overshoot in silicon, Solid-State Electron. 28 (1985) 407–416.
[19] C. Kittle, Introduction to Solid State Physics, John Wiley, New York, 1967.
[20] L.A. Falkovsky, E.G. Mishchenko, Electron-lattice kinetics of metals heated by ultrashort laser pulses, JETP 88 (1999) 84–88.

[21] L. Jiang, H.L. Tsai, Energy transport and material removal in wide bandgap materials by a femtosecond laser pulse, Int. J. Heat Mass Transfer 48 (2005) 487–499.
[22] J.K. Chen, W.P. Latham, J.E. Beraun, Axisymmetric modeling of femtosecond pulse laser heating on metal films, Numer. Heat Transfer A 42 (2002) 1–17.
[23] S.S. Wellershoff, J. Hohlfeld, J. Gudde, E. Matthias, The role of electron–phonon coupling in femtosecond laser damage of metals, Appl. Phys. A 69S (1999) 99–107.
[24] W.M.G. Ibrahim, H.E. Elsayed-Ali, C.E. Bonner Jr., M. Shinn, Ultrafast investigation of electron dynamics in multi-layer metals, Int. J. Heat Mass Transfer 47 (2004) 2261–2268.
[25] C.K. Sun, F. Vallee, L. Acioli, E.P. Ippen, J.G. Fujimoto, Femtosecond investigation of electron thermalization in gold, Phys. Rev. B 48 (1993) 12365–12368.
[26] J.K. Chen, W.P. Latham, J.E. Beraun, The role of electron–phonon coupling in ultrafast laser heating, J. Laser Appl. 17 (2005) 63–68.
[27] T.Q. Qiu, T. Juhasz, C. Suarez, W.E. Bron, C.L. Tien, Femtosecond laser heating of multi-layer metals—II. Experiments, Int. J. Heat Mass Transfer 37 (1994) 2799–2808.
[28] B.C. Stuart, M.D. Feit, S. Herman, A.M. Rubenchik, B.W. Shore, M.D. Peery, Optical ablation by high-power short-pulse lasers, J. Opt. Soc. Am. B 13 (1996) 459–468.